Molecular-dynamics modeling of Eu^{3+}-ion clustering in SiO_2 glass

N. D. Afify* and G. Mountjoy
School of Physical Sciences, University of Kent, Canterbury CT2 7NH, United Kingdom
(Received 18 September 2008; published 23 January 2009)

This paper reports a molecular-dynamics study on the clustering of Eu^{3+} ions incorporated in SiO_2 glass. Classical molecular-dynamics experiments were carried out on xEu_2O_3-$(100-x)SiO_2$ (x=0, 1, 2, 3, 4, and 5 mol %) glasses using empirical pairwise Morse interatomic potentials. Due to statistically improved simulation results, averaged over hundreds of Eu^{3+} ions, the effects of Eu_2O_3 content on the silica network, Eu^{3+} coordination, and on Eu^{3+} clustering were properly analyzed. At 1 mol % Eu_2O_3 most (~70%) of Eu^{3+} ions are isolated in silica host but have a strained coordination with typically three short bonds to nonbridging oxygens plus one long bond to bridging oxygen. It is found that the Eu^{3+}-O coordination number increases from 4.5 to 4.9 atoms due to an increase in sharing of nonbridging oxygens. This follows an increase in the Eu^{3+}-Eu^{3+} coordination number due to an increasing clustering of Eu^{3+} ions. Eu^{3+} clustering is already present in the sample with 1 mol % Eu_2O_3, but most of the clustered Eu^{3+} ions are present only in pairs. As Eu_2O_3 content increases in the glass, both the proportion of Eu^{3+} ions involved in clusters and the size of individual clusters increase, and signs of phase separation become apparent for 5 mol % Eu_2O_3.

DOI: 10.1103/PhysRevB.79.024202 PACS number(s): 61.43.Fs, 61.43.Bn, 81.05.Pj, 31.15.xv

I. INTRODUCTION

Glasses doped with trivalent rare-earth ions (RE^{3+}) are used in telecommunication systems as optical amplifiers. When fabricated in planar waveguiding format, these amplifiers are also used as integrated optical circuits, on which passive as well as active optical components are integrated. Thus, the dimensions of these devices should be as small as few centimeters in order to comply with integrated optics technology.[1] The cross section of the stimulated emission process of RE^{3+} ions, responsible for the optical amplification effect, is directly proportional to the content of the RE^{3+} ions in the host glass. Accordingly, in order to achieve high optical gain in such compact devices, large concentrations of the emitter ions (i.e., RE^{3+}) have to be homogeneously distributed in the host glass.

Unfortunately, RE^{3+} ions in glasses tend to form clusters at short distances of few angstroms and/or interact over large distances of about 20–100 Å.[2] In this paper we consider only the clustering of RE^{3+} ions. The concentration of RE^{3+} ions beyond which clustering occurs depends on the solubility of the host glass for the dopant ions. SiO_2 glass is one of the most important RE^{3+} hosts that are usually used in standard telecommunication applications.[1,3] It is known that SiO_2 glass shows quite poor solubility for RE^{3+} ions. This is due to the rigid nature of the tetrahedral SiO_2 network. The main effect of doping SiO_2 glass with RE^{3+} oxide is to introduce nonbridging oxygen (NBO) atoms. It is known that RE^{3+} ions are usually bonded to these NBOs for charge balance. Since a single RE^{3+} ion is charge balanced by just three NBOs, the available number of NBOs becomes insufficient to satisfy the coordination of homogeneously distributed dopant ions. Therefore, RE^{3+} ions tend to form clusters to share their oxygen coordination. Consequently, at high RE^{3+} contents, clustering of RE^{3+} ions is expected. This clustering is of great danger for the optical properties since it gives rise to a quenching of luminescence intensity by means of ion-ion interaction mechanisms.[2]

To enhance the solubility of RE^{3+} ions in SiO_2 glass, codoping with certain oxides has been widely explored. The presence of codopant oxide may increase the available number of NBOs in the material. This leads to a reduced probability of RE^{3+} ions clustering. To select systems with optimized functional properties, quantitative studies on RE^{3+} clustering in the different host materials are of fundamental importance. In a forthcoming paper, we will detail the mechanism by which the clustering of Eu^{3+} ions in silica glass is reduced by the addition of sodium oxide to the system.

Information on clustering of RE^{3+} ions in host glasses can be obtained from either spectroscopic or structural studies. Based on measured optical and spectroscopic properties, the presence of clustering of RE^{3+} ions can be observed. A detailed quantitative description of the clustering phenomena can be only derived from appropriate structural studies. From structural point of view, the clustering of RE^{3+} ions in the glass can be considered as the number of other RE^{3+} ions linked via oxygen to a given RE^{3+} ion. In structural terminology, this is in average the coordination number of the RE^{3+}-RE^{3+} partial correlation function. Unfortunately, experimental structural studies on RE^{3+}-doped glasses hardly provide such quantitative information.

Due to the fact that it is an average structure technique, x-ray diffraction (XRD) is not appropriate to study the clustering problem. This is explained by the fact that the content of RE^{3+} ions in the host glass is usually very small (e.g., few mol %). As a consequence, the dopant ions give negligible contribution to the total scattering patterns. Extended x-ray absorption fine structure (EXAFS), on the other hand, should be in principle the best experimental technique to study the clustering of RE^{3+} ions in glasses. Unfortunately, and to our knowledge, all EXAFS studies on RE^{3+}-doped glasses did not detect an already present RE^{3+}-RE^{3+} correlation (for recent review see Ref. 1). In glassy systems, coordination spheres beyond the first one are usually very disordered, and the large Debye-Waller factors due to this static disorder reduce the amplitude of correlations in the EXAFS spectra. For

this reason, RE^{3+}-RE^{3+} correlations, which first appear at distances of typically 4 Å, are difficult to detect in EXAFS data.

Molecular-dynamics (MD) simulation is a powerful technique able to yield detailed information on glass structure. Therefore, a quantitative description of the clustering of RE^{3+} ions in host glasses can, in principle, be efficiently obtained using this technique. The degree of success of MD simulation depends on a lot of factors. Among these are the reliability of the interatomic potentials, simulation methodology, and simulation box size. The last factor is extremely important for the current problem, where information related to the low-concentration dopant ions is the ones of interest.

Several MD results on RE^{3+}-doped glasses have been reported in literature. A common feature of these studies is the lack of any statistical assessment of the obtained results, particularly the ones related to RE^{3+} ions. For instance, in Refs. 4 and 5 Cormier *et al.* reported MD results on the structure of Eu^{3+}-doped SiO_2 and $xNa_2O.(100-x)SiO_2$ ($x=33$) glasses using simulation boxes containing only two Eu^{3+} ions. In Ref. 6, Du and Cormack simulated the structure of 1 mol % Er_2O_3 doped xNa_2O-$(99-x)SiO_2$ ($x=0$, 10, 20, and 30 mol %) and 2 mol % Er_2O_3-doped $30Na_2O70SiO_2$ glasses using simulation boxes containing 16 Er^{3+} ions. In the present paper we report the first MD results on xEu_2O_3-$(100-x)SiO_2$ ($x=0$, 1, 2, 3, 4, and 5 mol %) glasses, where the statistical reliability of the results is accounted for. The optimized simulation methodology allowed us to obtain original and statistically realistic information on the clustering of Eu^{3+} ions in Eu_2O_3-doped silica glass.

II. COMPUTATIONAL DETAILS

A. Interatomic potentials

Interatomic potentials, which describe forces acting on atoms during the course of MD experiments, are very important factors to optimize in order to obtain realistic MD structural results. In literature, there exist several quality potentials usually used to simulate the structure of vitreous SiO_2. In this work, we have assessed the relative accuracy of the following interatomic potentials: BKS Buckingham,[7] Vessal Buckingham,[8] Cormack Buckingham,[6] and Cormack Morse[9] potential parameters.

To find out the best interatomic potential we have carried out the following steps: (i) molecular-dynamics simulations on SiO_2 glass were performed using the different potential sets, (ii) the total static x-ray and neutron structure factors $S(Q)$ were calculated from the final MD atomic configurations, and (iii) direct comparisons between experimental and MD derived structure factors were made. It was found that the Cormack Morse interatomic potential parameters reported in Ref. 9 give the best agreement with experimental data. However, we found that the differences between results based on the different assessed interatomic potentials are always less than the overall deviation of MD results from experimental data.

The functional form of the interatomic potential used is written in Eq. (1). The three terms correspond, respectively, to (i) long-range Coulombic potential, (ii) short-range Morse potential with D_{ij}, a_{ij}, and r_0 are the potential parameters, and (iii) repulsive contribution $\frac{C_{ij}}{r^{12}}$, where C_{ij} is an adjustable parameter, necessary to model interactions at high temperatures and pressures. We have used partial ionic charges with the following values: $-1.2e$ for oxygen, $2.4e$ for silicon, and $1.8e$ for europium;

$$U(r) = \frac{(z_i z_j)e^2}{r} + D_{ij}[\{1 - e^{-a_{ij}\cdot(r-r_0)}\}^2 - 1] + \frac{C_{ij}}{r^{12}}. \quad (1)$$

TABLE I. Morse interatomic potential parameters for the $Si^{2.4}$-$O^{-1.2}$, $O^{-1.2}$-$O^{-1.2}$, and $Eu^{1.8}$-$O^{-1.2}$ atomic pairs.

Pair	D_{ij} (eV)	a_{ij} (Å^{-2})	r_0 (Å)	C_{ij} (eV Å)[a]
$O^{-1.2}$-$O^{-1.2}$	0.042395	1.379316	3.618701	22.0
$Si^{2.4}$-$O^{-1.2}$	0.340554	2.006700	2.100000	1.00
$Eu^{1.8}$-$O^{-1.2}$	0.000139	2.013200	4.351360	3.00

[a]Reference 12.

The potential parameters for $O^{-1.2}$-$O^{-1.2}$ and $Si^{2.4}$-$O^{-1.2}$ atomic pairs were taken from Ref. 9. The parameters for the $Eu^{1.8}$-$O^{-1.2}$ pair were refined starting from the parameters of the $Gd^{1.8}$-$O^{-1.2}$ pair reported in the same paper. The empirical refinement of these potential parameters was carried out using the general utility lattice program (GULP).[10] The refinement was performed at constant pressure (0.0 GPa), with no symmetry constraints applied. After obtaining reasonable potential parameters set using the "conventional fit" option, the experimental structures were relaxed[11] during the last cycles. The $Eu^{1.8}$-$O^{-1.2}$ potential parameters were varied until the crystal structure of the cubic Eu_2O_3 (Ref. 12) is very well reproduced. The resulting set of parameters was tested against the monoclinic[13] and orthorhombic[14] $Eu_2Si_2O_7$ crystal structures. Table I reports the final D_{ij}, a_{ij}, r_0, and C_{ij} values for the different atomic pairs.

Now we report on the accuracy of the interatomic potential parameters compiled in Table I. This kind of evaluation is usually done by comparing crystal structures predicted by potentials to the experimental ones, assuming therefore the transferability of these potentials to the disordered state. In Table II, we report the calculated and observed Eu^{3+}-O, Eu^{3+}-Eu^{3+}, Eu^{3+}-Si, and Si-O average interatomic distances in cubic europium oxide (c-Eu_2O_3),[12] orthorhombic europium disilicate (o-$Eu_2Si_2O_7$),[14] and monoclinic europium disilicate (m-$Eu_2Si_2O_7$).[13] As can be seen in Table II, the ability of the used potential to reproduce the observed crystal structures is quite fair. As expected, the agreement in the case of the simple-cubic structure is much better than the ones in the case of complex structures.

B. Simulation methodology

Classical MD simulation experiments were carried out using version 2.18 of the DLPOLY code.[15] The original code was modified by the present authors to systematically decrease the system temperature and therefore simulate the melt-quenching process which is responsible for forming the stud-

TABLE II. Calculated and observed Eu^{3+}-O, Eu^{3+}-Eu^{3+}, Eu^{3+}-Si, and Si-O average interatomic distances in *c*-Eu_2O_3 (Ref. 12), *o*-$Eu_2Si_2O_7$ (Ref. 14), and *m*-$Eu_2Si_2O_7$ (Ref. 13) crystalline structures based on the potential parameters in Table I. The coordination numbers (CNs) are also reported.

			Distance (Å)	
Crystal	Pair	CN atom	Observed	Calculated
c-Eu_2O_3	Eu^{3+}-O	6	2.3399	2.3419
	Eu^{3+}-Eu^{3+}	12	3.8554	3.8576
o-$Eu_2Si_2O_7$	Eu^{3+}-O	7	2.4038	2.4660
	Eu^{3+}-Eu^{3+}	5	4.1579	4.1388
	Eu^{3+}-Si	6	3.4048	3.4417
	Si-O	4	1.6239	1.5985
m-$Eu_2Si_2O_7$	Eu^{3+}-O	9	2.5406	2.5340
	Eu^{3+}-Eu^{3+}	7.5	4.1271	4.0884
	Eu^{3+}-Si	6	3.4216	3.5126
	Si-O	4	1.6267	1.6031

ied glasses in real experiments. The long-range Coulombic interactions were evaluated by the Ewald method,[16] using a real-space cutoff of 12.0 Å, and an Ewald precision factor of 10^{-5}. The short-range interaction cutoff was set to 7.6 Å. Integration of the Newton equations of motion was performed employing the Verlet Leapfrog algorithm[17] with a time step of 2 fs.

Each simulation experiment comprised six stages. In the first three stages, the system was equilibrated at the temperatures 6000, 3500, and 2200 K, each for 80 000 time step. In the fourth stage, the system was continuously quenched from 2200 to 300 K in 95 000 time step, having therefore a nominal quenching rate of 10^{13} K/s. In these four stages, velocities were scaled after each five time steps. In the fifth stage, the system was equilibrated at the room temperature for 80 000 time step. Finally, structural data were collected in the sixth stage each 50 time step, with a total of 1600 configurations.

In MD simulation of glass structure, it is very common to perform the simulation in constant *NVT* (i.e., number of particles *N*, system volume *V*, and temperature *T* are constants) conditions. In this case, the system is forced to have the experimental density of the real glass. Simulations of this kind often produce final atomic configurations with unrealistically huge pressures. Furthermore, we found that the magnitude and sign of this pressure depend, in fact, on the used interatomic potential. On the other hand, if the simulation is carried out in constant *NPT* (i.e., number of particles *N*, system pressure *P*, and temperature *T* are constants) conditions, the final pressures will be negligible, but the final density values will be different from the experimental ones. To judge which method yields more realistic structures, we carried out our simulations following two methodologies. In the first one, we have used the *NVT* canonical ensemble in all the simulation stages (we shall call this "*NVT* simulation"). In the second methodology, we used the *NVT* canonical ensemble during the high temperatures and quenching stages and the *NPT* canonical ensemble in the final two stages (we shall call this "*NPT* simulation"). For the *NVT* and *NPT* simulations, Berendsen thermostat and barostat were used, respectively, with a relaxation constant of 2 ps for each.

The number of atoms in the simulation box is a very important factor, particularly if we are looking for dopant-related structural information with high statistical quality. In fact, the main purpose of this paper is to study the clustering of Eu^{3+} ions, whose concentrations in the glass are small. We found that by repeating the same simulation, starting from different random configurations, peaks in the Eu^{3+}-Eu^{3+} pair distribution functions tend to have different positions in a randomlike way. To overcome this irreducibility problem, we have tried two different approaches. In the first one, we used a large number of Eu^{3+} ions (fixed to 50 ions for all samples) and repeated the simulation for three times, starting from different random configurations. In the second approach, we used small number of Eu^{3+} ions (greater than or equal to ten ions depending on the sample) and repeated the simulation for 25 times, starting in each time from different random configuration. From the computational point of view, the second approach is more efficient since the computation time required to carry out two simulations with *N* particles each is less than the time required to do a single simulation with 2*N* particles. By averaging the Eu^{3+}-Eu^{3+} pair distribution functions from the different repeats and by comparing the associated standard deviations, we concluded that the second methodology yields better statistics. In Table III, label, composition, density, and number of atoms in simulation box are reported for each sample.

III. RESULTS AND DISCUSSION

First we report on the validity of our simulation procedure by comparing the obtained MD structural results to experimental scattering data. This comparison can be carried out either in the real (*R*) or reciprocal (*Q*) spaces. It is more common in literature to compare the computational and experimental data in the real space. However, sometimes authors apply an arbitrary broadening to MD derived real-space correlation functions in order to enhance agreement with experiment. This may be due to the lack of the original experimental scattering data (i.e., structure factors) and information on the way these data were transformed into the real space. A more rigorous comparison between experimental and MD scattering data should be carried out in reciprocal space, where Fourier transformation and its consequences are avoided. A part from that, it is also important to do such comparison with more than one data set, i.e., both x-ray and neutron-scattering data.

Here we compare the computational and experimental structural data for SiO_2 glass (sample S0). A comparison for Eu^{3+}-doped SiO_2 glasses was not made due to the lack of experimental scattering data. Moreover, doping SiO_2 with such few mol % Eu_2O_3 would give only tiny effects on the diffraction pattern of silica glass. In Fig. 1, we report a comparison between experimental (solid black spheres) and MD based x-ray (lower curves) and neutron (upper curves) scattering interference functions $Q.i(Q)$. The MD spectra are shown for both *NVT* (dotted blue lines) and *NPT* (continuous

TABLE III. Label, composition, density, and number of atoms in the simulation box for each sample. All Eu^{3+}-containing models were repeated 25 times each, while for model S0 the simulation was repeated only for five times.

Sample label	Eu_2O_3 (mol %)	SiO_2 (mol %)	Density (g/cm^3)	No. of atoms		
				Si	O	Eu
S0	0	100	2.200	1000	2000	0
S1	1	99	2.287	495	1005	10
S2	2	98	2.374	490	1010	20
S3	3	97	2.461	469	980	28
S4	4	96	2.548	468	996	40
S5	5	95	2.634	456	984	48

red lines) simulation methodologies. While neutron data were extracted from Grimley *et al.*,[18] x-ray data were collected on the BM08 GILDA beamline of the European Synchrotron Radiation Facility (ESRF).

As can be seen from Fig. 1 the agreement between the experimental and MD results is quite fair. The evident superior agreement in the case of neutron data can be due to the following reasons: (i) x-ray scattering data are richer with information on medium range order (MRO) and (ii) in neutron scattering, the atomic nuclei are the scattering objects which are closer to what happens in MD experiments. The comparison between the *NVT* and *NPT* simulation results reveals a slightly better agreement in the case of *NPT* dynamics.

In order to discriminate the relative goodness of *NVT* and *NPT* simulation procedures, we report the results relative to bond angle distributions in SiO_2 glass. The Si-O-Si and O-Si-O bond angle distributions calculated from *NVT* (dotted blue lines) and *NPT* (continuous red lines) MD results are reported in Fig. 2. The distributions maxima are evidenced by vertical dotted lines.

From Fig. 2, it can be seen that the *NPT* simulation predicts a Si-O-Si bond angle distribution that has a full width at half maximum (FWHM) of 37.5° and a mean angle of 147.8°. The mean value of the Si-O-Si bond angle predicted by *NVT* simulation is 152.4°. The experimental value of the mean Si-O-Si bond angle has been reported based on diffraction data by Mozzi and Warren[19] as 147.9° and recently by Neuefeind and Liss[20] as 146.7°. From this result and the fact that the agreement with the scattering data is slightly better in the case of *NPT* simulation, we conclude that the quality of *NPT* simulation is better than the *NVT* one. Therefore, our decision to carry out *NVT* simulation followed by *NPT* dynamics at the end of simulation is now justified. As for the O-Si-O bond angle distribution, both *NVT* and *NPT* simulations give a mean angle of 107.9° and a FWHM of 14.5°, which is in agreement with experimental values reported in Ref. 21.

Before we report our MD structural results on $x Eu_2O_3$-$(100-x)SiO_2$ (x=0, 1, 2, 3, 4, and 5 mol %) glasses, we define in Fig. 3 the different kinds of oxygen species present in these glasses. Ideally, pure SiO_2 network (sample S0) is fully composed of corner-shared SiO_4 tetrahedral units. In this case, each silicon is bonded to two oxygen, and each oxygen is bonded to two silicon atoms (see Fig. 3). Let us denote this kind of oxygen bridging oxygen (BO). When they are introduced into SiO_2 glass, RE^{3+} ions create oxygen atoms that are bonded only to one silicon. Let us call this kind of oxygen NBO. In principle, each NBO can

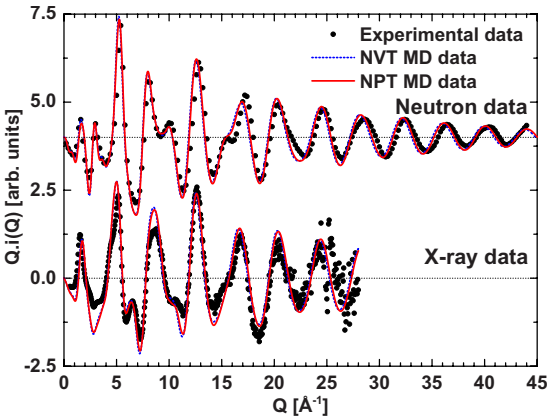

FIG. 1. (Color online) Experimental (solid black spheres) versus *NVT* (dotted blue lines) and *NPT* (continuous red lines) MD derived x-ray (lower curves) and neutron (upper curves) scattering interference functions $Qi(Q)$ for SiO_2 glass (sample S0).

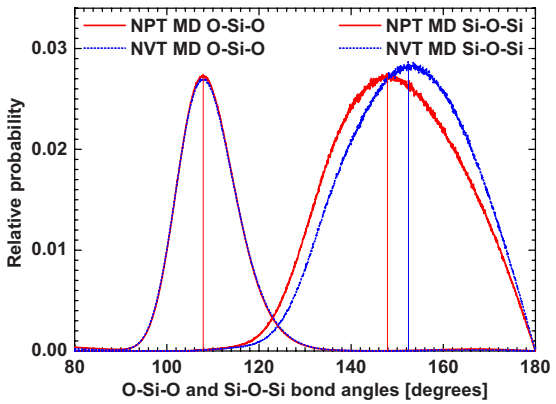

FIG. 2. (Color online) The O-Si-O and Si-O-Si bond angles distributions in SiO_2 glass (sample S0), as calculated from *NVT* (dotted blue lines) and *NPT* (continuous red lines) MD results. Distributions maxima are evidenced by vertical dotted lines.

FIG. 3. Classification of the different types of oxygen atoms in Eu^{3+}-doped SiO_2 glasses.

be bonded to one europium ion (we shall call it NBO^*) or to two europium ions (we shall call it NBO^{**}). Some of the BOs can also be bonded to one europium ion (we shall call it BO^*).

A. Depolymerization of SiO_2 network

In this section, we report and discuss the effects of doping with Eu^{3+} on the structure of SiO_2 network in xEu_2O_3-$(100-x)SiO_2$ (x=0, 1, 2, 3, 4, and 5 mol %) glasses. Figure 4(a) reports the Si-O, O-O, and Si-Si partial real-space correlation functions of SiO_2 network for samples S0 (continuous black lines) and S5 (dotted red lines). For sample S0 each spectrum is an average over five independent simulations, while for all the Eu^{3+}-containing samples the averages were taken over 25 independent simulations. From this figure we note that doping with 5 mol % Eu_2O_3 has very slight effects on the total Si-O, O-O, and Si-Si correlations. This is due to the fact that these effects are masked by the "untouched" parts of silica network, which remains dominant. However, in the following paragraphs we highlight the changes which are occurring. Structural parameters, such as average coordination numbers N, average interatomic distances R, and FWHMs, characterizing the first peaks in these correlations are compiled in Table IV.

The effects of doping with 5 mol % Eu_2O_3 on the Si-O, O-O, and Si-Si peaks are documented in Fig. 4(a). In fact, the three peaks of sample S5 exhibit lower amplitudes compared to the ones of sample S0. This can be caused by reductions in coordination numbers and/or disordering in these coordination shells. This situation is clarified in Table IV, where the quantitative results are reported. From this table, it can be seen that doping with Eu^{3+} ions induces reductions in both O-O and Si-Si coordination numbers, while the average coordination number of Si-O correlation is not affected. The presence of Eu^{3+} ions in SiO_2 network induces also slight disordering into the Si-O and ordering into O-O and Si-Si coordination spheres, as evidenced by the FWHM values in Table IV. Very slight contractions in the Si-O and O-O average distances and expansion in Si-Si average distance can also be observed. The structural changes are too small to be experimentally observed but are caused by changes to the SiO_2 network due to the incorporation of Eu^{3+} ions, as the following paragraphs discuss.

Figure 4(b) reports the Si-O coordination shell as a sum of two contributions: a dominant contribution (continuous lines) coming from the Si-BO bonds and a small one (dotted lines) coming from the Si-NBO bonds. For clarity, the contribution Si-NBO was magnified ten times. As expected, by

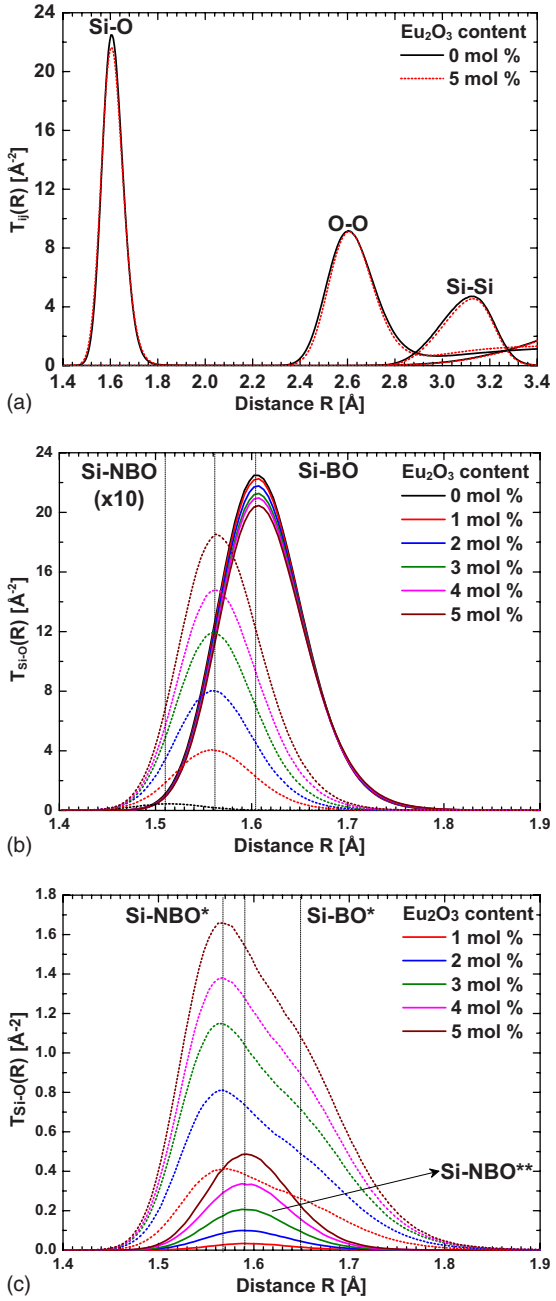

FIG. 4. (Color online) MD derived partial real-space correlation functions $T_{ij}(R)$ of SiO_2 glass as a function of Eu_2O_3 content. (a) The Si-O, O-O, and Si-Si correlations for the samples S0 (continuous black lines) and S5 (dotted red lines). (b) The Si-BO (continuous lines) and magnified Si-NBO (dotted lines) contributions to the Si-O correlation. (c) The $Si\text{-}NBO^{**}$ (continuous lines) and $Si\text{-}NBO^*+Si\text{-}BO^*$ (dotted lines) contributions to the Si-O correlation.

increasing Eu_2O_3 content in the glass, the number of NBOs increases at the cost of the number of BOs. This explains the increase in the Si-NBO contribution at the cost of the Si-BO one. An important result in Fig. 4(b) is the shortening of the Si-NBO average distance with respect to the one of Si-BO. This result can be interpreted in the light of the bond valence theory[22] as follows. Since the Eu^{3+}-O coordination number is typically 6, then the bond valence of a Eu^{3+}-NBO bond is

TABLE IV. Average coordination numbers N, average interatomic distances R, and FWHMs characterizing the first peaks in the Si-O, O-O, and Si-Si partial correlation functions for samples S0 and S5.

Correlation	N (atom)	R (Å)	FWHM (Å)
Si-O (S0)	4.00	1.613	0.102
Si-O (S5)	4.00	1.612	0.106
O-O (S0)	6.16	2.632	0.228
O-O (S5)	5.77	2.630	0.213
Si-Si (S0)	4.02	3.094	0.262
Si-Si (S5)	3.71	3.097	0.249

$v=0.5$. The remaining bond valence of a NBO is in the Si-NBO bond. Since the Si-NBO bond will have bond valence of $v=1.5$, then the Si-NBO distance is shorter relative to the normal Si-BO bond, which has bond valence of $v=1.0$.

In Fig. 4(c), we classify more contributions to the Si-O coordination shell. Here we are interested only in the oxygen species that are involved in bonding with Eu^{3+} ions. In this figure, three components of Si-O bonds, related to three different kinds of oxygen atoms, can be identified: (i) oxygen bonded to two silicon and one Eu^{3+} ion (the contribution Si-BO*), (ii) oxygen bonded to one silicon and one Eu^{3+} ion (the contribution Si-NBO*), and (iii) oxygen bonded to one silicon and two Eu^{3+} ions (the contribution Si-NBO**). As expected, the amplitudes of these contributions increase as a function of Eu_2O_3 content. In this figure, it can also be noted the shortening of the Si-NBO* distance with respect to the Si-NBO** one. This result can be interpreted as follows. If a NBO is bonded to two Eu^{3+} ions and each Eu^{3+}-NBO bond has bond valence of $v=0.5$, the NBO will have a remaining bond valence of $v=1.0$ which is in the Si-NBO bond. This bond will then be of the same length as a normal Si-BO bond with bond valence of $v=1.0$. The elongation of the Si-BO* bond with respect to the Si-NBO** one can be explained in similar way.

The depolymerization of SiO_2 network, by doping, can be efficiently described through the analysis of Q^n species in the glass. In Fig. 5, distributions of the Q^n ($n=2$, 3, and 4) species in SiO_2 glass as a function of Eu_2O_3 content are reported. Here, Q^2, Q^3, and Q^4 refers, respectively, to silicon atoms coordinated by 2, 3, and 4 BOs. The creation of NBOs means that the silica network is no longer 100% Q^4. Each NBO created will convert one Q^4 into a Q^3. Thus, we see that the Q^4 decrease is almost balanced by the Q^3 increase, so that Q^3 plus Q^4 is nearly 100%. It is theoretically possible that the creation of two NBOs would convert a Q^4 into a Q^2, however the amount of Q^2 is seen to be small in Fig. 5. In fact, in silicate glasses it is known that there is preferential disassociation from Q^n to Q^{n-1} and not from Q^n to Q^{n-2}.

B. Local structure around Eu^{3+} ions

Now we move the attention to the local structure around Eu^{3+} ions in the simulated glasses. In Eu^{3+}-doped SiO_2 glasses, oxygen, silicon, and europium atoms are the constituent atoms of the first, second, and third coordination shells around Eu^{3+} ions, respectively. The partial Eu^{3+}-O and Eu^{3+}-Si correlation functions are shown in Fig. 6(a), and the Eu^{3+}-Eu^{3+} ones are reported in Fig. 6(d). Table V reports the average interatomic distance of the Eu^{3+}-O shell ($\langle R_{Eu^{3+}\text{-}O}\rangle$), Eu^{3+}-O peak width (FWHM), $N_{Eu^{3+}\text{-}BO^*}$, $N_{Eu^{3+}\text{-}NBO*}$, and $N_{Eu^{3+}\text{-}NBO**}$ contributions to Eu^{3+}-O coordination number and Eu^{3+}-Si coordination number as a function of Eu_2O_3 concentration. The cutoff values for the Eu^{3+}-O, Eu^{3+}-Si, and Eu^{3+}-Eu^{3+} correlations were set at 3.0, 4.2, and 5.0 Å.

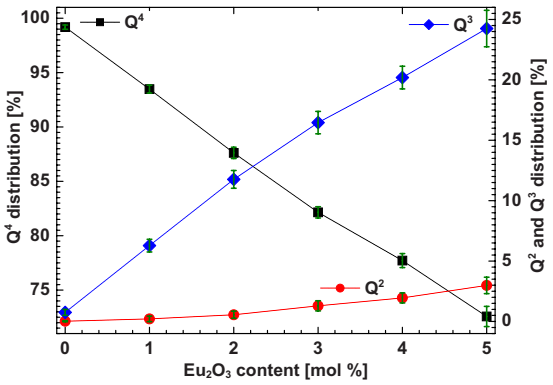

FIG. 5. (Color online) Distributions of the Q^n ($n=2$, 3, and 4) species in silica glass as a function of Eu_2O_3 content.

From Fig. 6(a), we note that the Eu^{3+}-Si peaks are centered around 3.65 Å. This coordination shell is independent of Eu_2O_3 content. In fact, for Eu_2O_3 concentrations ranging from 1 to 5 mol %, it is found that europium ions are always coordinated by approximately six silicon atoms (see Table V). As we have discussed, Eu^{3+} ions are bonded to both NBOs and BOs, and these oxygen atoms are themselves bonded to Si. It is clear that each NBO is bonded to a different Si. Eu^{3+} ions are not expected to be edge shared with Si, which is not favorable for +3 and +4 cations, so for each BO there are expected to be another two Si as next-nearest neighbors of Eu^{3+}. Table V shows that this is true since $N_{Eu^{3+}\text{-}NBO}+2N_{Eu^{3+}\text{-}BO^*}\simeq N_{Eu^{3+}\text{-}Si}$. Note that $N_{Eu^{3+}\text{-}NBO}=N_{Eu^{3+}\text{-}NBO^*}+N_{Eu^{3+}\text{-}NBO^{**}}$.

The coordination numbers found in the present study vary from 4.5 for the S1 to 4.9 for S5 glasses (Table V). In previous modeling studies of RE^{3+} dopants in pure SiO_2 glass, Cormier *et al.*[5] found a coordination number of 4 for 1 mol % Eu^{3+} and Du and Cormack[6] found a coordination number of 4.9 for 1 mol % Er^{3+}. These values are similar to the value of 4.4 for S1 glass in the present study. In addition, the study of Du and Cormack[6] shows that the Er^{3+} coordination number increases toward 6 as Na_2O is added to SiO_2 glass. The value of 6 is significant because this is the lowest RE^{3+} coordination found in crystalline materials. All these results are consistent with a RE^{3+} coordination number significantly below 6 in pure SiO_2 glass due to the limited availability of NBOs when modifier cations such as Na are absent. In previous EXAFS studies of 1–4 mol % RE^{3+} dopants in SiO_2, Rocca *et al.* found values of 6 ± 1 for Tb^{3+} (Ref. 23) and 6.0 ± 0.7 for Er^{3+} (Ref. 24) in SiO_2. These experimental values can be consistent with a coordination number below 6 in pure SiO_2.

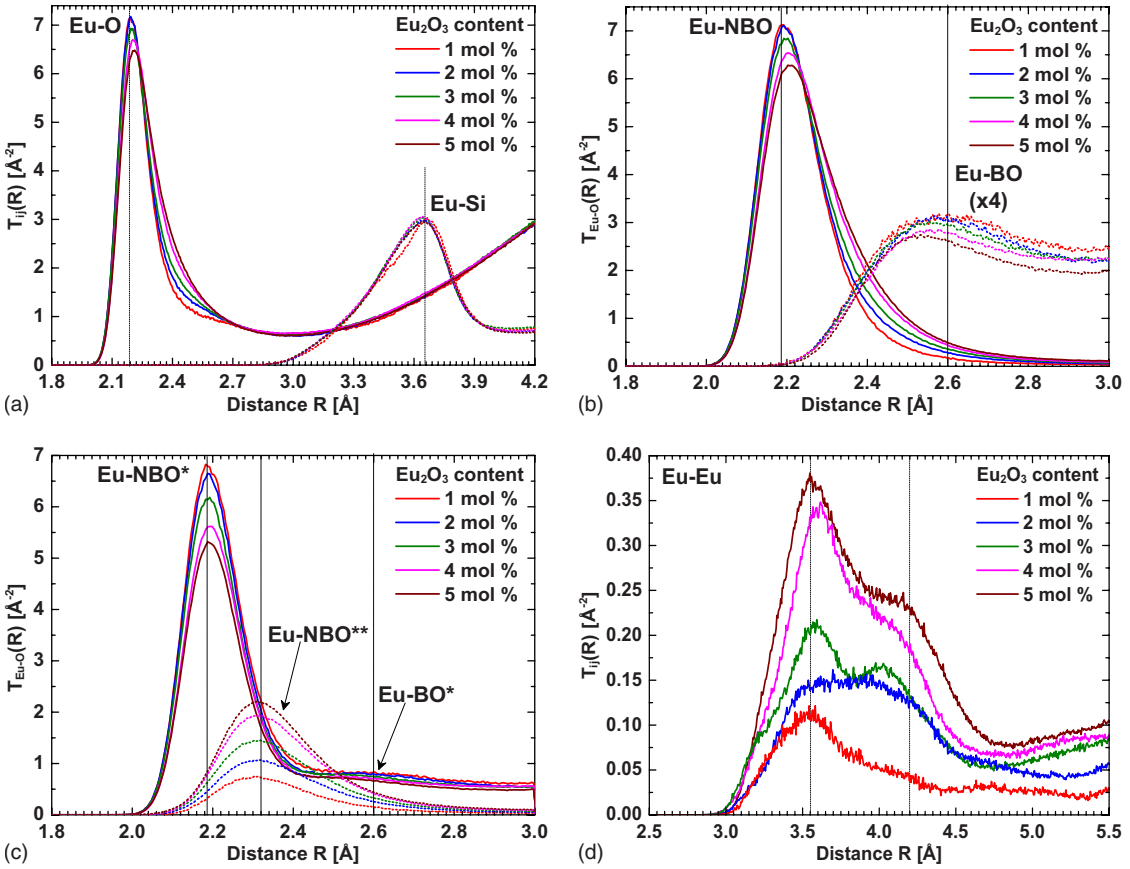

FIG. 6. (Color online) MD derived partial real-space correlation functions $T_{ij}(R)$ around Eu^{3+} ions in SiO_2 glass as a function of Eu_2O_3 content. (a) The Eu^{3+}-O (continuous lines) and Eu^{3+}-Si (dotted lines) correlations. (b) The Eu^{3+}-BO (dotted lines) and magnified Eu^{3+}-NBO (continuous lines) contributions to the Eu^{3+}-O correlations. (c) The Eu^{3+}-NBO^{**} (dotted lines) and Eu^{3+}-NBO^{*}+Eu^{3+}-BO^{*} (continuous lines) contributions to the Eu^{3+}-O correlations. (d) The Eu^{3+}-Eu^{3+} correlations.

The Eu^{3+}-O partial correlation functions, reported in Fig. 6(a), show strongly asymmetric distributions centered around 2.19 Å. It can be depicted from this figure and Table V that the average interatomic distance, peak width, and degree of asymmetry increase as a function of Eu_2O_3 content. It can also be seen that the area under the Eu^{3+}-O peak increases, reflecting an increasing coordination number as a function of Eu_2O_3 concentration.

The average interatomic distances reported in Table V were taken as peak centroid. Here we justify why we have considered the peak centroid instead of peak maximum for the average interatomic distance calculations. For Eu^{3+}-O coordination shell, strong asymmetry is an important feature of the correlation function, having therefore large differences between the peak maximum and centroid for all samples. It is very common in literature to consider the peak maximum when reporting average interatomic distances. This however leads to very short distances, which deviate significantly from the experimental values. That is the reason why we have chosen the peak centroid instead. The resulting values of distances are closer to the maximum of a symmetric Gaussian distribution function to which EXAFS data are

TABLE V. The average interatomic distance of the Eu^{3+}-O shell ($\langle R_{Eu^{3+}\text{-}O}\rangle$), Eu^{3+}-O peak width (FWHM), $N_{Eu^{3+}\text{-}BO*}$, $N_{Eu^{3+}\text{-}NBO*}$, and $N_{Eu^{3+}\text{-}NBO**}$ contributions to Eu^{3+}-O coordination number, and Eu^{3+}-Si coordination number as a function of Eu_2O_3 concentration. The cutoff values for the Eu^{3+}-O, Eu^{3+}-Si, and Eu^{3+}-Eu^{3+} correlations were set at 3.0, 4.2, and 5.0 Å.

Sample label	$\langle R_{Eu^{3+}\text{-}O}\rangle$ (Å)	$FWHM_{Eu^{3+}\text{-}O}$ (Å)	$N_{Eu^{3+}\text{-}NBO*}$ (atom)	$N_{Eu^{3+}\text{-}NBO**}$ (atom)	$N_{Eu^{3+}\text{-}BO*}$ (atom)	$N_{Eu^{3+}\text{-}Si}$ (atom)
S1	2.333	0.183	2.6(1)	0.7(3)	1.2(2)	5.9(1)
S2	2.337	0.187	2.7(2)	0.7(3)	1.1(2)	5.9(1)
S3	2.344	0.195	2.4(1)	1.2(2)	1.1(1)	6.0(1)
S4	2.354	0.213	2.2(2)	1.4(2)	1.1(1)	6.0(1)
S5	2.357	0.227	2.2(2)	1.5(2)	1.1(2)	5.9(1)

usually fitted. In fact, our Eu^{3+}-O average interatomic distances are in good agreement with EXAFS results reported in Ref. 25.

A deeper understanding of the Eu^{3+}-O coordination shell is accessible only by analyzing the different components of this shell. Thanks to the superior details of molecular dynamics over experimental structural techniques, the different kinds of oxygen atoms contributing to a certain coordination shell can be analyzed separately. Figure 6(b) presents the Eu^{3+}-NBO (continuous lines) and magnified Eu^{3+}-BO (dotted lines) components of the Eu^{3+}-O coordination shell.

As mentioned above, Eu^{3+} should be coordinated by at least three NBOs, and each of these is coordinated to one Si. It is very unlikely that Eu^{3+} would be coordinated by two NBOs coming from the same Si since that would create Q^2 species. In addition, it would also mean that Eu^{3+} and Si ions form edge sharing, which is not favorable in this case. However, Eu^{3+} is a medium-sized ion and cannot exist with such low coordination of three (due to three NBOs). Therefore, it must raise its coordination to 4 or higher. One way it can do this is by bonding also to BOs.

As it is shown in Fig. 3, oxygen atoms bonded to europium ions in the first coordination shell (i.e., Eu^{3+}-O) can be classified in a different way. Figure 6(c) shows the Eu^{3+}-NBO^{**} (dotted lines) and Eu^{3+}-NBO^{*}+Eu^{3+}-BO^{*} (continuous lines) contributions to the Eu^{3+}-O coordination shell. The corresponding coordination numbers are reported in Table V. From both Fig. 6(c) and Table V one can realize that as the Eu_2O_3 content increases in the glass, the fraction of europium ions sharing the same oxygen increases at the cost of the fraction of europium ions sharing no oxygens with each other. This is an important result since it is related directly to the increase in clustering of RE^{3+} ions as their number increases in the host glass.

In addition, Table V shows that the $N_{Eu^{3+}\text{-}BO*}$ coordination number is roughly constant ($\simeq$1 atom), instead the $N_{Eu^{3+}\text{-}NBO}$ coordination number, which is $N_{Eu^{3+}\text{-}NBO*}+N_{Eu^{3+}\text{-}NBO**}$, increases with Eu_2O_3 concentration. This can be explained as follows. If Eu^{3+} ion is isolated, the three NBOs it creates are the only NBOs available, and the $N_{Eu^{3+}\text{-}NBO}$ coordination number must be limited to 3. However, if there is another Eu^{3+} ion nearby, this Eu^{3+} ion itself has NBOs, and it is possible that they can be shared with the other Eu^{3+} ion. For example, two neighboring Eu^{3+} ions, each with three NBOs and each sharing one of their NBOs with the other Eu^{3+}, will have $N_{Eu^{3+}\text{-}NBO}$ coordination number of 4. Table V shows that the $N_{Eu^{3+}\text{-}NBO}$ coordination number increases from 3 to 4 by increasing Eu_2O_3 concentration, and this is exactly due to sharing of NBOs among nearby Eu^{3+} ions. We shall refer to this as "clustering" of Eu^{3+} ions.

Coming back to Fig. 6(c), we note that the Eu^{3+}-O interatomic distance increases from Eu^{3+}-NBO^{*} to Eu^{3+}-NBO^{**} and then to Eu^{3+}-BO^{*}. This behavior can be understood using the same principle as discussed for Si-O bonds. It is known that the interatomic distance gets longer as the bond valence gets lower. For a NBO^{*} in Si-NBO^{*} bond, there remains a large amount of bond valence for the Eu^{3+}-NBO^{*} bond, and the Eu^{3+}-NBO^{*} distance is very short. For a NBO^{**} this valence is divided between two Eu^{3+} ions, and so the Eu^{3+}-NBO^{**} distance gets longer. For a BO^{*} with two Si-BO^{*} bonds, there remains a very little bond valence for Eu^{3+}-BO^{*} bond, and so the Eu^{3+}-BO^{*} distance gets very long.

More important are the results on the Eu^{3+}-Eu^{3+} coordination shell which are reported in Fig. 6(d). For sample S1, a single peak centered around 3.55 Å can be observed. As Eu_2O_3 concentration increases, another peak centered around 4.20 Å develops. By increasing Eu_2O_3 content in the glass, the Eu^{3+}-Eu^{3+} distributions become broader, and the area under the Eu^{3+}-Eu^{3+} peak progressively increases. This shows an increasing clustering effect of Eu^{3+} ions. It is interesting to compare the distance between and number of Eu^{3+}-Eu^{3+} neighbors in the glass with typical values from $Eu_2Si_2O_7$ crystals (see Table II). The distances are similar because in both the crystal and the glass, Eu^{3+}-Eu^{3+} neighbors are connected through oxygen atoms as mediators. However, as expected, dilution in the glass causes the number of Eu^{3+}-Eu^{3+} neighbors to be very much smaller than in the crystals, as will be seen in Sec. III C.

C. Evaluation of Eu^{3+} ion clustering in SiO_2 glass

Now we focus on evaluating and understanding the clustering of europium ions incorporated in silica glass. As we anticipated in the introductory part, structural information on Eu^{3+} clustering can be derived from the RE^{3+}-RE^{3+} partial correlation function. Although of its great importance, this correlation function has been hardly quantified and commented in most of the published MD results. This is probably due to poor statistical quality of simulation results, which in turn is due to the limited numbers of dopant ions usually used the simulation box.[6]

Our Eu^{3+}-Eu^{3+} partial correlation function is plotted in Fig. 6(d) for the different Eu_2O_3 contents. Thanks to the optimized simulation methodology, the shown spectra are of high statistical quality compared to the ones published in literature. It can be noticed that the Eu^{3+}-Eu^{3+} distribution function is very broad, reflecting a very disordered nature of this coordination shell. This probably is the main reason why the present RE^{3+}-RE^{3+} correlation is not detectable by EXAFS measurements.[1,23,24,26–30]

Figure 7(a) shows both the Eu^{3+}-O (black solid squares) and Eu^{3+}-Eu^{3+} (red solid spheres) coordination numbers as a function of Eu_2O_3 content. Expectedly, the trend of the Eu^{3+}-Eu^{3+} coordination number shows an increasing clustering effect. Figure 7(a) shows that as Eu_2O_3 content increases in the glass, the Eu^{3+}-O coordination number increases from a bit larger than four to almost five oxygen atoms. This corresponds to an increase in the number of NBO^{**} (i.e., oxygen atoms that are bonded to two europium ions), and consequently there is a proportionate increase in the Eu^{3+}-Eu^{3+} coordination number, i.e., Eu^{3+}-NBO^{**}-Eu^{3+} linkages. This means a greater likelihood of nearby Eu^{3+} ion, which we have referred to as clustering.

The Eu^{3+}-O coordination numbers reported in Fig. 7(a) are average values. It is expected that some europium ions will be coordinated by three, four, or five oxygen atoms. In addition to the average Eu^{3+}-O coordination numbers, it is

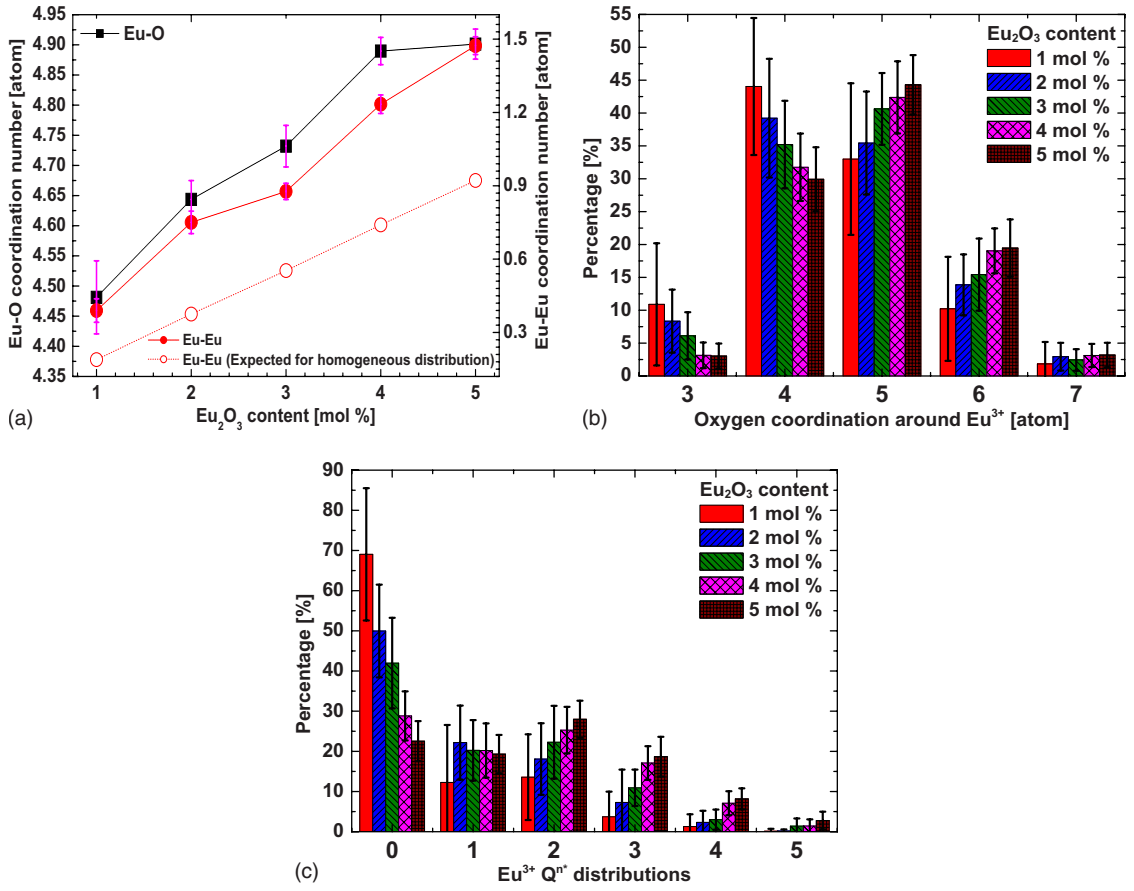

FIG. 7. (Color online) Coordination numbers around Eu^{3+} ions in SiO_2 glass as a function of Eu_2O_3 content. (a) The Eu^{3+}-O (black solid squares) and Eu^{3+}-Eu^{3+} (red solid spheres) coordination numbers. The Eu^{3+}-Eu^{3+} coordination numbers expected for homogeneous distribution of Eu^{3+} ions (red empty spheres) are shown for comparison. (b) Distributions of oxygen coordination around Eu^{3+} ions. (c) Distributions of the Eu^{3+} Q^n (n=0, 1, 2, 3, 4, and 5) species.

useful to study the distribution of oxygen coordination around Eu^{3+} ions. Figure 7(b) reports the percentages of three-, four-, five-, six-, and seven-oxygen coordinated Eu^{3+} ions. As a function of Eu_2O_3 content, this figure shows clearly that the fraction of europium ions coordinated by three and four oxygen atoms decreases, while the fraction of europium ions coordinated by five and six oxygen atoms increases. This trend shows the clustering evolution as a function of Eu_2O_3 content.

At this point, based only on the reported Eu^{3+}-Eu^{3+} coordination numbers let us demonstrate the presence of clustering between europium ions in our simulated glasses. Let us assume that Eu^{3+} ions are homogeneously distributed, and we need to know the average number of Eu^{3+} ions per unit volume of the structures. If N is the number of Eu^{3+} ions in a cubic box of edge L (Å), then the atomic number density is $\rho=N/L^3$ ion/Å^3. Let us now consider the model with 1 mol % Eu_2O_3, 50 Eu^{3+} ions, and L=47.7 Å [the model shown in Fig. 8(a)]. This gives $\rho=0.46\times10^{-3}$ ion/Å^3. Now, if we choose a spherical volume of space $V=\frac{4}{3}\pi R^3$, then the average number of Eu^{3+} ions we should have inside (for a homogeneous distribution) is $V\rho$. If we consider a central Eu^{3+} ion and a "nearest-neighbor distance" of R_{max}, then we can estimate the number of "neighboring" Eu^{3+} ions, as per the previous formula. However, we should exclude the volume very close to the central Eu^{3+} ion since we know that it is occupied by oxygen atoms. We define this by a minimum distance R_{min}.

Looking at the Eu^{3+}-Eu^{3+} correlation functions reported in Fig. 6(d), we see that R_{min}=3.0 Å and R_{max}=5.0 Å. The calculation gives $V_{shell}=\frac{4}{3}\pi R_{max}^3-\frac{4}{3}\pi R_{min}^3=410.5$ Å^3. Using this value of V_{shell} with ρ from above gives that the number of Eu^{3+} ions per unit volume of the structure is $V_{shell}\rho$ =0.19 ion. So, on average there would be 0.19 neighboring Eu^{3+} around a central Eu^{3+} ion. Since there can be either zero or one neighboring ion, this could be interpreted as 19% of Eu^{3+} ions have one Eu^{3+} neighbor and 81% of Eu^{3+} ions have zero Eu^{3+} neighbor. The 1 mol % model has number of Eu^{3+}-Eu^{3+} neighbors equal to 0.39, so this is significantly higher than the one expected for a homogeneous distribution and shows that there is an additional "force" which makes Eu^{3+} more likely to be neighbors. We repeat the calculations for the model with 5 mol % Eu_2O_3, 50 Eu^{3+} ions, and L =28.1 Å [the model shown in Fig. 8(e)]. This gives ρ =2.25×10^{-3} ion/Å^3. Therefore, the number of Eu^{3+} ions is $V_{shell}\rho$=0.92 ion. Thus, 92% of Eu^{3+} ions have one Eu^{3+} neighbor and 8% of Eu^{3+} ions have zero Eu^{3+} neighbor. Since the model with 5 mol % has number of Eu^{3+}-Eu^{3+} neighbors equal to 1.47, then we have high degree of Eu^{3+} clustering. The number of Eu^{3+}-Eu^{3+} neighbors expected for

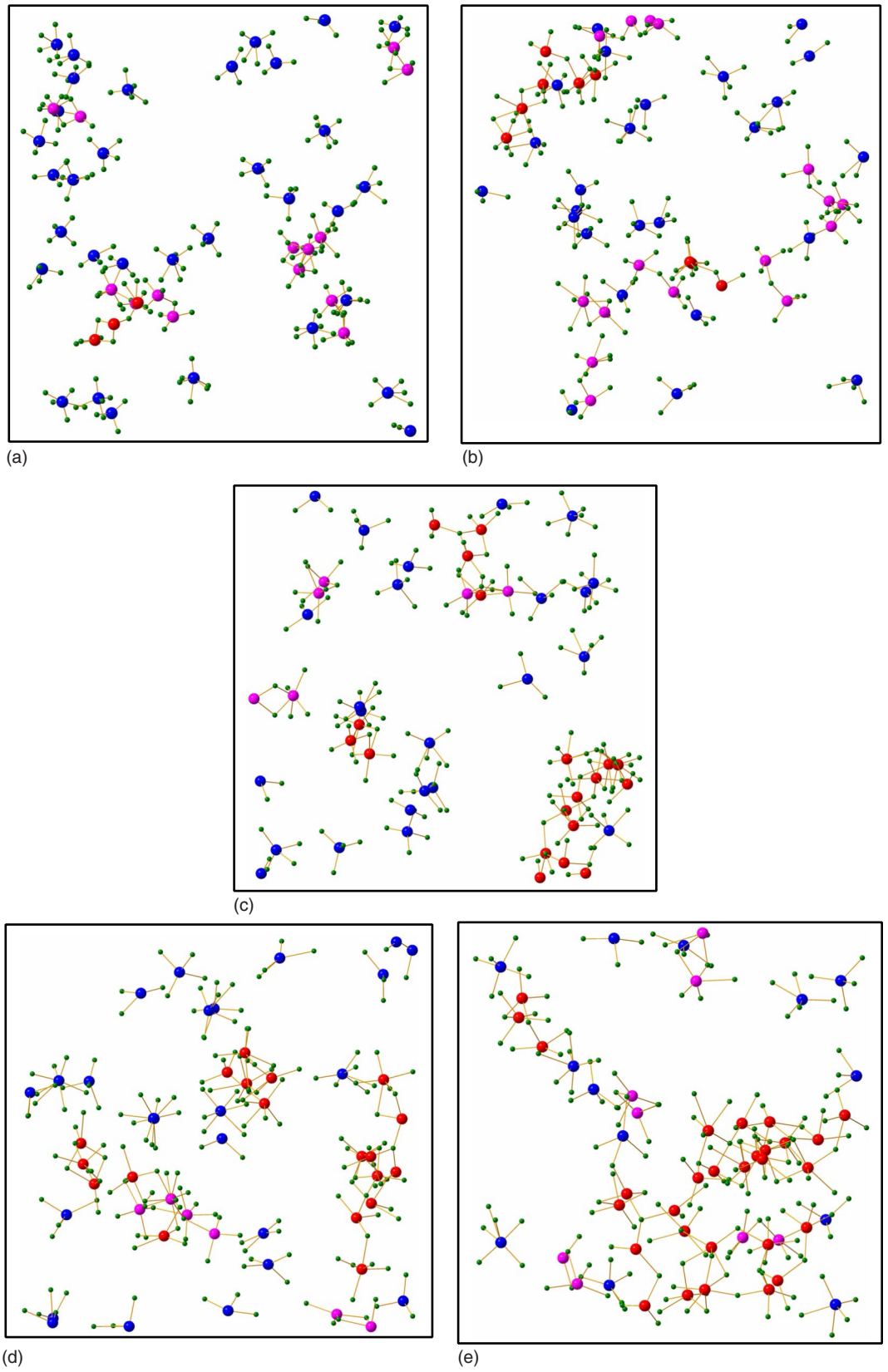

FIG. 8. (Color online) Illustration of clustering of Eu^{3+} ions in xEu_2O_3-$(100-x)SiO_2$ (x=1, 2, 3, 4, and 5 mol %) glasses [(a), (b), (c), (d), and (e), respectively]. The shown images correspond to MD simulations with 50 Eu^{3+} ions in each simulation box. For clarity, only Eu^{3+} ions and their nearest neighbors of oxygen atoms are shown. The green (small), blue (dark gray), magenta (light gray), and red (medium gray) spheres refer, respectively, to O, isolated Eu^{3+}, Eu^{3+} bonded to single Eu^{3+} ion, and Eu^{3+} bonded to more than one Eu^{3+} ion.

homogeneous distribution of Eu^{3+} ions is reported for all the studied compositions in Fig. 7(a). Expectedly, as the content of Eu_2O_3 increases in the glass, the deviation between the actual Eu^{3+}-Eu^{3+} coordination numbers and the ones expected for homogeneous distributions increases.

Finally, we classify Eu^{3+} ions according to the number of nearby Eu^{3+} ions, using the Q^n notation, which is normally used for Si network. Figure 7(c) shows the distribution of these Q^n (n=0, 1, 2, 3, 4, and 5) species. In this figure, Q^0, Q^1, Q^2, Q^3, Q^4, and Q^5 refer to the percentage of europium ions that have connections to other 0, 1, 2, 3, 4, and 5 europium ions, respectively. This figure confirms that for the sample with 1 mol % Eu_2O_3, most (~70%) of Eu^{3+} ions are isolated, but by increasing Eu_2O_3 content the majority of Eu^{3+} ions become parts of clusters. This is expected since the SiO_2 glass offers very limited solubility for Eu^{3+} ions. In fact, the Eu_2O_3-SiO_2 phase diagram shows that for 5 mol % Eu_2O_3, phase separation is expected to occur.

MD simulation is a very powerful technique to study clustering of RE^{3+} ions not only by resorting to the calculated coordination numbers but also by inspecting the final atomic configurations. Clustering of Eu^{3+} ions in xEu_2O_3-(100 $-x$)SiO_2 (x=1, 2, 3, 4, and 5 mol %) glasses is illustrated by the final simulation images in Fig. 8. The shown images correspond to MD simulations with 50 Eu^{3+} ions in each simulation box. For clarity, only Eu^{3+} ions and their nearest neighbors of oxygen atoms are shown. In this figure, the green (small), blue (dark gray), magenta (light gray), and red (medium gray) spheres refer, respectively, to O, Eu^{3+} bonded to no Eu^{3+}, Eu^{3+} bonded to only one Eu^{3+}, and Eu^{3+} bonded to more than one Eu^{3+} ion.

Now we compare the systems with 1 mol % [Fig. 8(a)] and 2 mol % [Fig. 8(b)] Eu_2O_3. In the former, Eu^{3+} ions are mostly isolated, some of them are present in pairs, and very few of them are involved in clusters containing more than two Eu^{3+} ions. In the latter system, the number of ions involved in nonpaired clusters increased. From Figs. 8(c)–8(e), it is evident that as the concentration of Eu_2O_3 increases, both the number and size of nonpaired clusters increase. Therefore, the evolution of Eu^{3+} clustering as a function of Eu_2O_3 content can be described by the following mechanisms: (i) the number of Eu^{3+} ions involved in clusters increase and (ii) Eu^{3+} clusters grow in size.

IV. CONCLUSIONS

In this paper, detailed and statistically improved molecular-dynamics results on the structure of xEu_2O_3-(100$-x$)SiO_2 (x=0, 1, 2, 3, 4, and 5 mol %) glasses are reported. The effects of Eu_2O_3 content on Eu^{3+} clustering and on the structure of SiO_2 glass were properly quantified. For the system with 1 mol % Eu_2O_3, clustering of Eu^{3+} ions is already present, but most of the clustered ions are present in pairs. Increasing Eu_2O_3 concentration in the glass enhances the present clustering by the following mechanisms: (i) the number of Eu^{3+} involved in clusters increases and (ii) the average size of individual Eu^{3+} clusters increases. The reported computational study shows the reason why the present RE^{3+}-RE^{3+} correlations in RE^{3+}-doped glasses are not usually detected by EXAFS measurements. Due to the strong chemical similarity among the rare earths, the insights detailed in this paper for Eu^{3+} ions should also be relevant for understanding the effects of doping SiO_2 with other RE^{3+} ions.

ACKNOWLEDGMENTS

We are grateful for funding from the UK Engineering and Physical Sciences Research Council (EPSRC). N.D.A. would like to thank A. N. Cormack, G. Dalba, F. Rocca, and M. Alfredsson for useful discussions on results. Authors are grateful to C. Meneghini for providing x-ray diffraction data on SiO_2 glass.

*n.afify@kent.ac.uk

[1] N. D. Afify, G. Dalba, C. Armellini, M. Ferrari, F. Rocca, and A. Kuzmin, Phys. Rev. B **76**, 024114 (2007).
[2] E. Desurvire, *Erbium-Doped Fiber Amplifiers: Principles and Applications* (Wiley, New York, 1994).
[3] N. Afify, G. Dalba, and F. Rocca (unpublished).
[4] G. Cormier, J. Capobianco, and A. Monteil, J. Non-Cryst. Solids **152**, 225 (1993).
[5] G. Cormier, J. A. Capobianco, C. A. Morrison, and A. Monteil, Phys. Rev. B **48**, 16290 (1993).
[6] J. Du and A. Cormack, J. Non-Cryst. Solids **351**, 2263 (2005).
[7] B. W. H. van Beest, G. J. Kramer, and R. A. van Santen, Phys. Rev. Lett. **64**, 1955 (1990).
[8] B. Vessal, M. Amini, D. Fincham, and C. R. A. Catlow, Philos. Mag. B **60**, 753 (1989).
[9] A. Pedone, G. Malavasi, M. Menziani, A. Cormack, and U. Segre, J. Phys. Chem. B **110**, 11780 (2006).
[10] J. Gale and A. Rohl, Mol. Simul. **29**, 291 (2003).
[11] J. D. Gale, Philos. Mag. B **73**, 3 (1996).
[12] Z. Heiba, Y. Akin, W. Sigmund, and Y. Hascicek, J. Appl. Crystallogr. **36**, 1411 (2003).
[13] M. Fleet and X.-Y. Liu, J. Solid State Chem. **161**, 166 (2001).
[14] J. Felsche, Struct. Bonding (Berlin) **13**, 99 (1973).
[15] W. Smith and T. R. Forester, J. Mol. Graphics **14**, 136 (1996).
[16] P. P. Ewald, Ann. Phys. **64**, 253 (1921).
[17] M. Allen and D. Tildesley, *Computer Simulation of Liquids* (Clarendon, Oxford, 1991).
[18] D. Grimley, A. Wright, and R. Sinclair, J. Non-Cryst. Solids **119**, 49 (1990).
[19] R. Mozzi and B. Warren, J. Appl. Crystallogr. **2**, 164 (1969).
[20] J. Neuefeind and K.-D. Liss, Ber. Bunsenges. Phys. Chem. **100**, 1341 (1996).
[21] S. von Alfthan, A. Kuronen, and K. Kaski, Phys. Rev. B **68**, 073203 (2003).
[22] I. D. Brown, Acta Crystallogr., Sect. B: Struct. Crystallogr. Cryst. Chem. **33**, 1305 (1977).

[23] F. Rocca, F. Monti, A. Kuzmin, A. Dalmaso, and D. Pasqualini, J. Synchrotron Radiat. **6**, 737 (1999).
[24] F. Rocca, C. Armellini, M. Ferrari, G. Dalba, N. Diab, A. Kuzmin, and F. Monti, J. Sol-Gel Sci. Technol. **26**, 267 (2003).
[25] L. Županc-Mežnar, R. Cerc-Korošec, P. Bukovec, and J. Padežnik Gomilšek, J. Vac. Sci. Technol. B **18**, 1097 (2000).
[26] F. Rocca, M. Ferrari, A. Kuzmin, N. Daldosso, C. Duverger, and F. Monti, J. Non-Cryst. Solids **293-295**, 112 (2001).
[27] N. Afify, R. Grisenti, G. Dalba, C. Armellini, M. Ferrari, S. Larcheri, F. Rocca, and A. Kuzmin, Opt. Mater. **28**, 864 (2006).
[28] F. d'Acapito, S. Mobilio, L. Santos, and R. M. Almeida, Appl. Phys. Lett. **78**, 2676 (2001).
[29] F. d'Acapito, S. Mobilio, P. Gastaldo, D. Barbier, L. F. Santos, O. Martins, and R. M. Almeida, J. Non-Cryst. Solids **293-295**, 118 (2001).
[30] C. Maurizio, F. D'Acapito, F. Priolo, G. Franzò, F. Iacona, E. Borsella, S. Padovani, and P. Mazzoldi, Opt. Mater. **27**, 900 (2005).